Arch. Metall. Mater. **66** (2021), 1, 153-161

DOI: 10.24425/amm.2021.134771

ZHEN SHANG[1†], YINGYING ZUO[1†], SHUDE JI[1*], YUE WANG[2**], PENG CHAI[2]

JOINT FORMATION AND MECHANICAL PROPERTIES OF 2060 ALUMINUM ALLOY REFILL FRICTION STIR SPOT WELDING JOINT

Refill friction stir spot welding (RFSSW) was used to weld the 2060 aluminum alloy with 2 mm thickness. Joint formation, defect characteristics and mechanical properties were investigated. Results show that stir zone (SZ) is clarified into dynamic recrystallization zone (DRZ) and heat extruded zone (HEZ) due to different microstructural features. The size of void near the hook tip decreases with the increase of the plunge depth. Different hook morphologies are obtained under different plunge depths. The tensile-shear load of joint with the void defect initially decreases and then increases with increasing plunge depth. The mean loads of joints under different plunge depths are in the range of 5.1-5.8 kN. The void separates the hook from lap interface, so the cracks initiating from the hook propagate along the sleeve retreating path. The hook has a larger influence on the tensile-shear load of joint than void. All the tensile specimens present a shear-plug fracture mode.

Keywords: Refill friction stir spot welding, 2060 aluminum alloys, plunge depth, defect characteristics, mechanical properties

1. Introduction

Aluminum lithium alloys are widely used in aerospace due to high specific strength and specific stiffness, excellent corrosion resistance and fatigue crack propagation resistance [1-2]. As a new type of aluminum lithium alloys, 2060-T8 aluminum alloy is used as a skin material and has been identified as an excellent candidate to replace 2024 aluminum alloy [3-5]. Lap joining is the main way to connect skin and beam. However, the fusion welding technologies such as resistance spot welding easily cause pore and hot crack inside weld [6]. Mechanical connections such as riveting increase the structural weight and decrease the connection efficiency because of drilling prior to welding. Thus, mechanical connections are also not a good choice to join aluminum lithium alloys.

Friction stir spot welding (FSSW) is a relatively new solid-state welding technology [7-8] in which peak temperature is lower than melting point of material, what allows for avoiding the defects in fusion welding technologies. To date, FSSW has been used in the RX-8 automobile rear wheels and some structures of Toyota Motor [9]. However, the remained keyhole in the FSSW joint decreases the efficient bearing-load area, thereby causing stress concentration and decreasing tensile-shear load of joint. Refill friction stir spot welding (RFSSW), a variant of FSSW, attains a welding joint without a keyhole by relative motions of sleeve and pin [10].

de Castro et al. [11] optimized the RFSSW parameters for 1.6 mm thick 2198-T8 aluminum lithium alloy using Taguchi approach, and found that rotational speed and plunge depth were responsible for more than 80% of strength variance. A similar result has been reported in 5042 aluminum alloy RFSSW joint [12]. The presented RFSSW of 2198-T8 aluminum lithium alloy showed the effect of plunge depth [13] or rotational speed [14] on the microstructure and mechanical properties of joint. The investigation of 6061-T6 aluminum alloy RFSSW demonstrated that plunge depth had an important influence on the morphology and height of hook near the lap interface, and the larger hook height generated smaller lap shear strength of RFSSW joint [15]. Hook is an inherent characteristic in the lap joint, and it cannot be eliminated by optimization of process parameters. In addition, void, incomplete welding and crack are the critical factors to affect mechanical properties of joint. However, to the best of our knowledge, there are no published studies addressing the investigation of relation between hook, welding defects and

[1] SHENYANG AEROSPACE UNIVERSITY, COLLEGE OF AEROSPACE ENGINEERING, SHENYANG 110136, CHINA
[2] BEIHANG UNIVERSITY, SCHOOL OF MECHANICAL ENGINEERING AND AUTOMATION, BEIJING, 100083, CHINA

Corresponding authors: * superjsd@163.com; ** endlesswy@163.com

† Yingying Zuo and Zhen Shang contributed equally to this work

mechanical properties of joint, as well as those factors accounting for the variant of mechanical properties.

This work aims to study the primary factors to affect the mechanical properties of 2 mm thick 2060-T8 aluminum lithium alloy welded by RFSSW under different sleeve plunge depths, and it points out which factor is the main reason to influence tensile-shear load of RFSSW joint.

2. Experiments

2 mm thick 2060-T8 aluminum lithium alloy was chosen as the welded material in this study, and its chemical compositions were 0.72% Li, 0.025% Si, 0.026% Fe, 3.56% Cu, 0.3% Mn, 0.72% Mg, 0.34% Zn, 0.086% Ag and balanced Al (all in wt%). The heat treatment of this material was T8 condition, namely, solution heat treatment, cold work and artificial aging. The specimens with 140 mm (length) × 30 mm (width) × 2 mm (thickness) were used for lap-shear tests with an overlap area of 30 mm × 45 mm, as shown in Fig. 1. The welding spot was located at the center of the overlap area. The welding experiments were performed using Robotic RFSSW-RS01-06 equipment assembled by Beijing FSW Technology Co, Ltd. The welding tool included a clamping ring, sleeve and pin, and their external diameters were 18, 9 and 6 mm, respectively. The rotational speed of 2500 rpm, plunge rate of 60 mm/min and refill rate of 60 mm/min were fixed during the welding process, and the variable plunge depths were 2.4, 2.6, 2.8 and 3 mm. The metallographic specimens were cut, grinded, polished and etched along the center of the welding spot. Finally, the cross section and microstructure of each joint were observed using a light microscope (LM). The testing hardness was microhardness, and the metallographic specimens after observing the microstructures were used to measure the microhardness. The microhardness was measured using an HVS-1000 Vickers hardness tester with a pyramid indenter. Testing locations were the cross sections of the metallographic specimens. The testing force of 10 gf, dwell time of 10 s, a testing space of 0.5 mm were used during the testing process. The tensile-shear tests were conducted according to the ISO 14273 standard. The fracture locations of tensile-shear specimens were observed using the LM.

3. Results and discussion

3.1. Formation analysis

Fig. 2 shows the cross sections of joints under different plunge depths. Obviously, the upper and lower sheets were successfully joined, and the keyhole was not observed. For the RFSSW joint, the cross section was divided into stir zone (SZ), thermo-mechanically affected zone (TMAZ), heat affected zone (HAZ) and base material (BM). Several researchers divided the SZ into sleeve affected zone (SAZ) and pin affected zone (PAZ) on the basis of different mechanical actions of the welding tool [13]. From the cross sections in Fig. 2, the microstructures in the SZ parallel and perpendicular to the sheet thickness were rather uneven. The material adjacent to the sleeve and pin consisted of fine dynamic recrystallization grains due to severe mechanical action and high temperature. This region was regarded as dynamic recrystallization zone (DRZ) in this study, as marked in Fig. 2a. During the welding process material surrounded by the DRZ was squeezed into the sleeve at the plunging stage and extruded out of the sleeve at the refilling stage. This part of material which did not come to contact with the sleeve and pin only suffered extrusion at high temperature, and this region was named as heat extruded zone (HEZ), as marked in Fig. 2a. Note that DRZ and HEZ both existed in all the RFSSW joints under different plunge depths in Fig. 2.

Zones inside and outside the DRZ possess different morphologies, thereby leading to difference in microstructure parallel and perpendicular to the sheet thickness in the whole joint. These zones mainly include sleeve retreating path and lap interface, and these two zones are weak regions for the joints. Fig. 2b shows the partitions of two zones. Zones 1 is the BM; Zone 2 and 3 are located at the bottom of the DRZ; Zones 4 and 5 are located at the DRZ of the upper sheet; Zone 6 is the lap interface just below the pin; Zones 7 and 8 are the microstructures along the path of sleeve retreating.

Fig. 3 shows the microstructures of different Zones in Fig. 2b. The BM presents the elongated lath-shaped microstructure along the rolling direction in Fig. 3a. The microstructure distributions in the sleeve retreating path (Figs. 3b, 3c, 3d and 3e) and lap interface (Fig. 3f) are identical, which are characterized by SZ, TMAZ and HAZ. The bending degree of microstructure

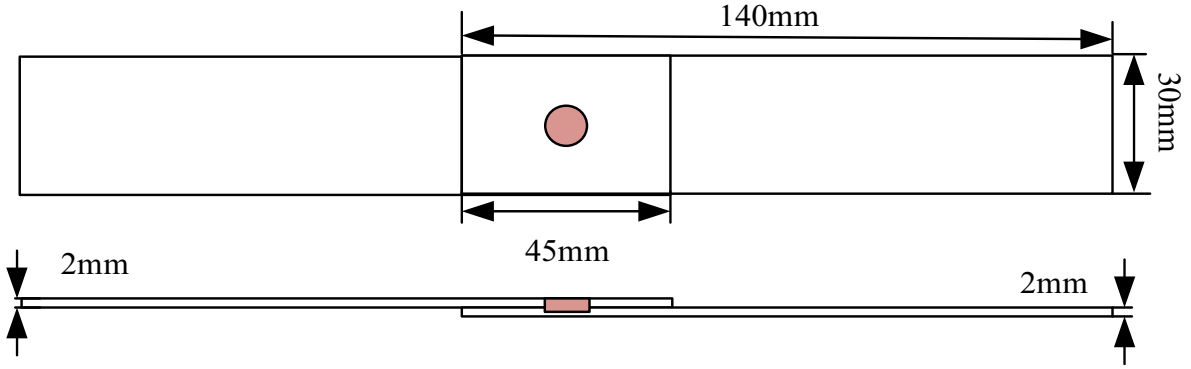

Fig. 1. Schematic of the lap-shear specimen

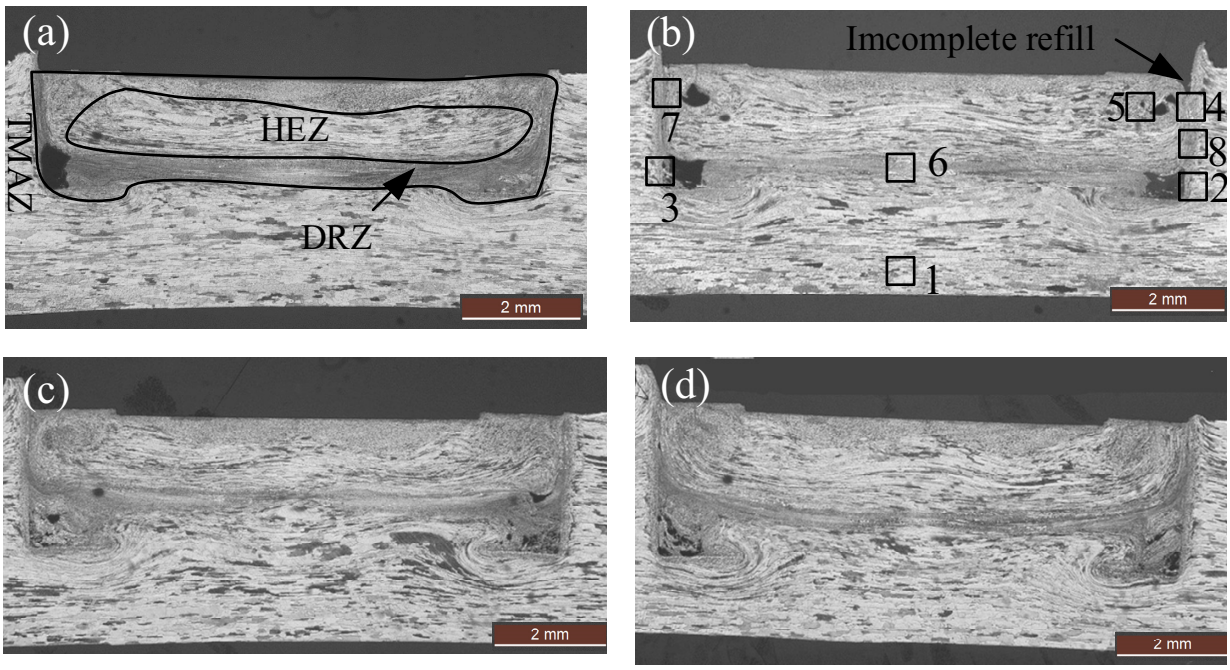

Fig. 2. Cross sections of joints under different plunge depths: (a) 2.4, (b) 2.6, (c) 2.8 and (d) 3 mm

in TMAZ at the bottom of the DRZ (Fig. 3d) is larger than that in the sleeve retreating path (Fig. 3b). The microstructure of TMAZ in the lap interface is squeezed and presents elongated along the rolling direction, and it in the path of sleeve retreating bends along the thickness. Figs. 3g and 3h show the microstructures of the DRZ. The DRZ in different locations (Fig. 2a) consists of fine equiaxed grains, and several grains occur bending. Different microstructures in different zones have various influences on the mechanical properties of joints, which is discussed in the following part.

3.2. Defect characteristics

Fig. 4 shows the magnified images of the bottom of the sleeve retreating path under different plunge depths. The void defect was observed at each welding condition, and it was located at the bottom of the sleeve retreating path and at the tip of the hook. Size of a single void defect at low plunge depths (2.4 and 2.6 mm) were large (Figs. 4a and 4b). With increasing plunge depth, the size of the single void decreased, but the whole size of void was still large (Figs. 4c and 4d).

Hook was observed at each cross section. Hook was attributed to the bending of lap interface when the sleeve plunged into the lower sheet [16-17]. Parra et al. [18] pointed out that the hook with upside down "V" shape in the 6181-T4 aluminum alloy RFSSW joint was due to the plastic deformation of the lower sheet, and the hook geometry was associated with heat input. Shen et al. [19-20] reported that the hook morphology was related to the physical properties of materials. The hook presents upward and downward bending morphologies under different plunge depths in this study. The downward and upward hooks are regarded as H_1 and H_2, respectively. When the plunge depths are in the range of 2.4-2.8 mm, the hook bends downward, and the bending degree gradually increases with the increase of plunge depth, as shown in Figs. 4a-4c. When the plunge depth increases to 3 mm, the hook turns to bend upward, as marked in Fig. 4d.

The causes of hook formation are complicated, which combines with material flow, heat input, and thermophysical properties of materials around hook. It is incomplete to explain the hook formation using a single reason. The heat input increases with increasing plunge depth during the welding process, thereby leading to the decreased material viscosity. Hence, much more materials are driven downward with increased plunge depth. Meanwhile, material near the bottom of the sleeve driven by the sleeve increases at the plunging stage, and the material flow becomes better. These factors decrease the void along the sleeve retreating path when the plunge depth increases. When the plunge depth reaches 3 mm, the material viscosity decreases too small to drive material. On the contrary, the material in the lap interface is squeezed by the SZ material to bend upward.

Fig. 5 shows the microstructures of lap interfaces below the pin under different plunge depths. It is obvious that all the lap interfaces are completely joined. Although the material in the lap interface do not closely contact with the pin, the microstructure of the lap interface presents fine grains. This part of material belongs to DRZ as mentioned above, and it has been marked in Fig. 5. During the plunging stage, the material squeezed into the sleeve and below the pin occurs in situ deformation when the sleeve plunges into the lap sheets. With the refilling of the rotational pin, this part of material occurs diffusion bonding under the extrusion of the rotational pin. Therefore, the material above the lap interface is squeezed to form the elongated lath-shaped structure, and this is also the microstructure of HEZ, as marked in Fig. 5. The material below the lap interface presents the coarsened grains, and the coarsened grains is regarded as the HAZ.

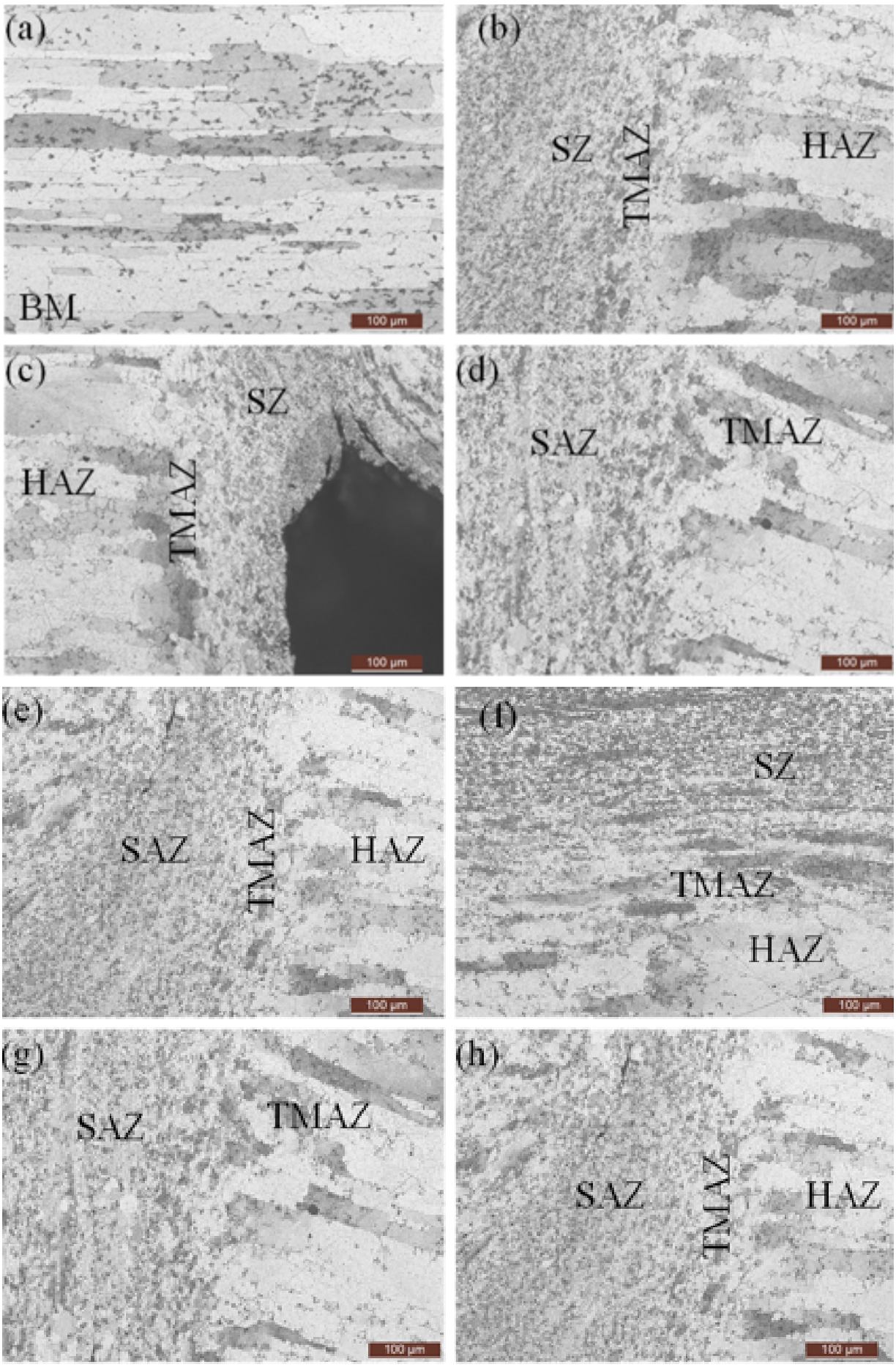

Fig. 3 Microstructures in Fig. 1a: (a) Zone 1, (b) Zone 2, (c) Zone 3, (d) Zone 4, (e) Zone 5, (f) Zone 6, (g) Zone 7and (h) Zone 8

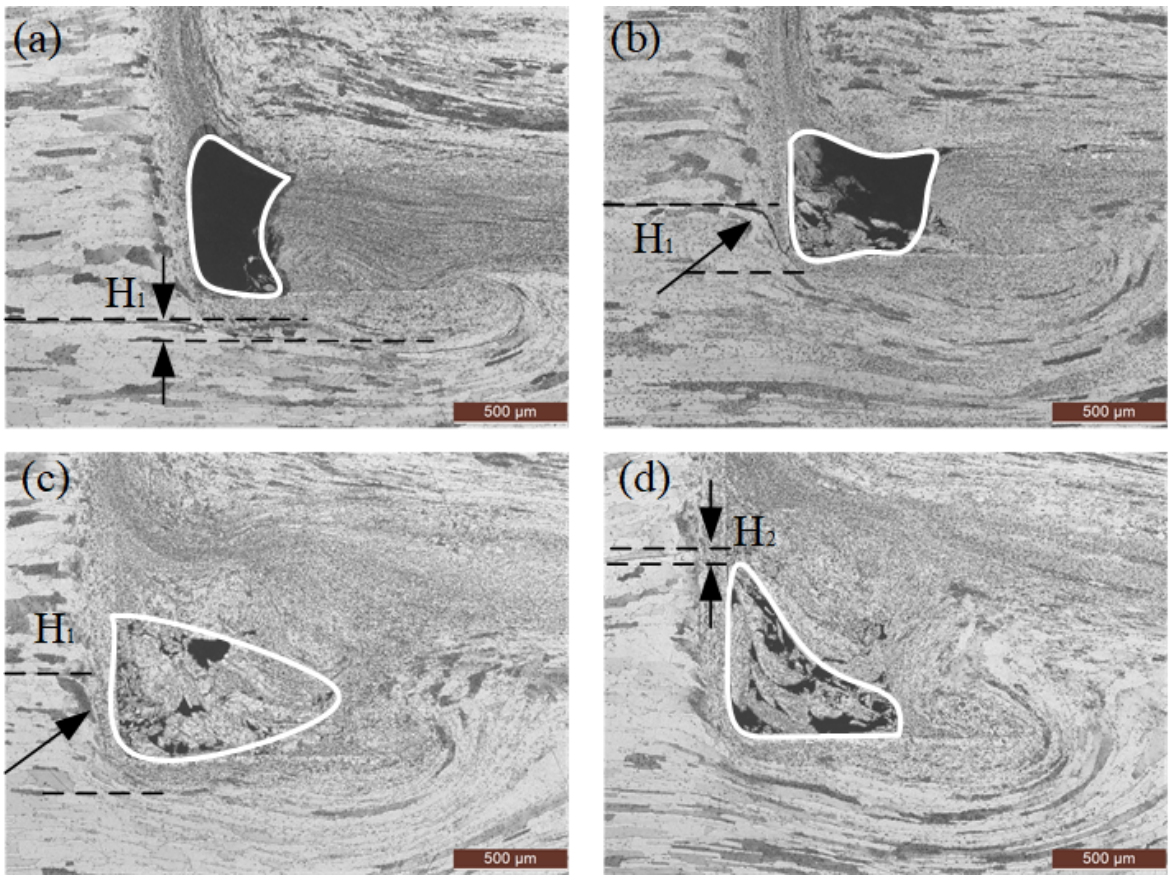

Fig. 4. Defect characteristics of joints under different plunge depths: (a) 2.4, (b) 2.6, (c) 2.8 and (d) 3 mm

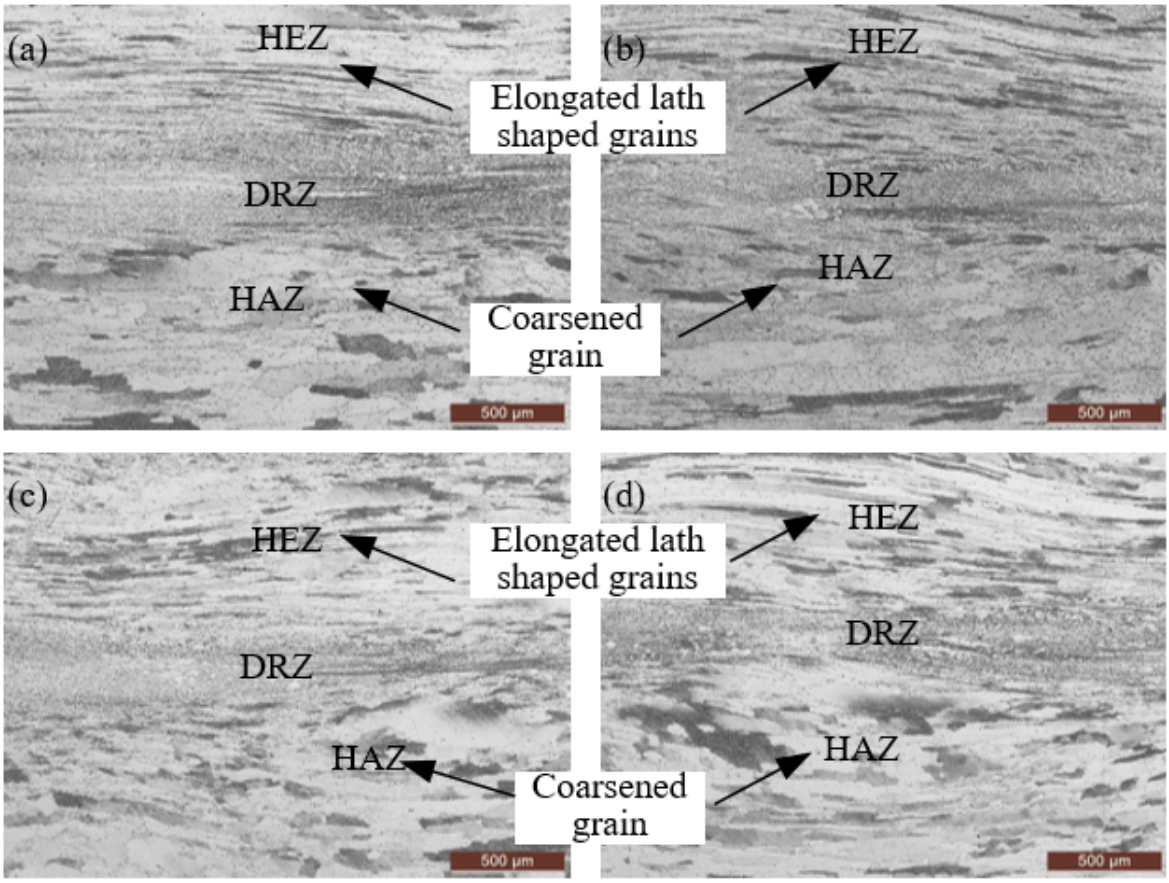

Fig. 5. Microstructures of joints lap interfaces below the pin under different plunge depths: (a) 2.4, (b) 2.6, (c) 2.8 and (d) 3 mm

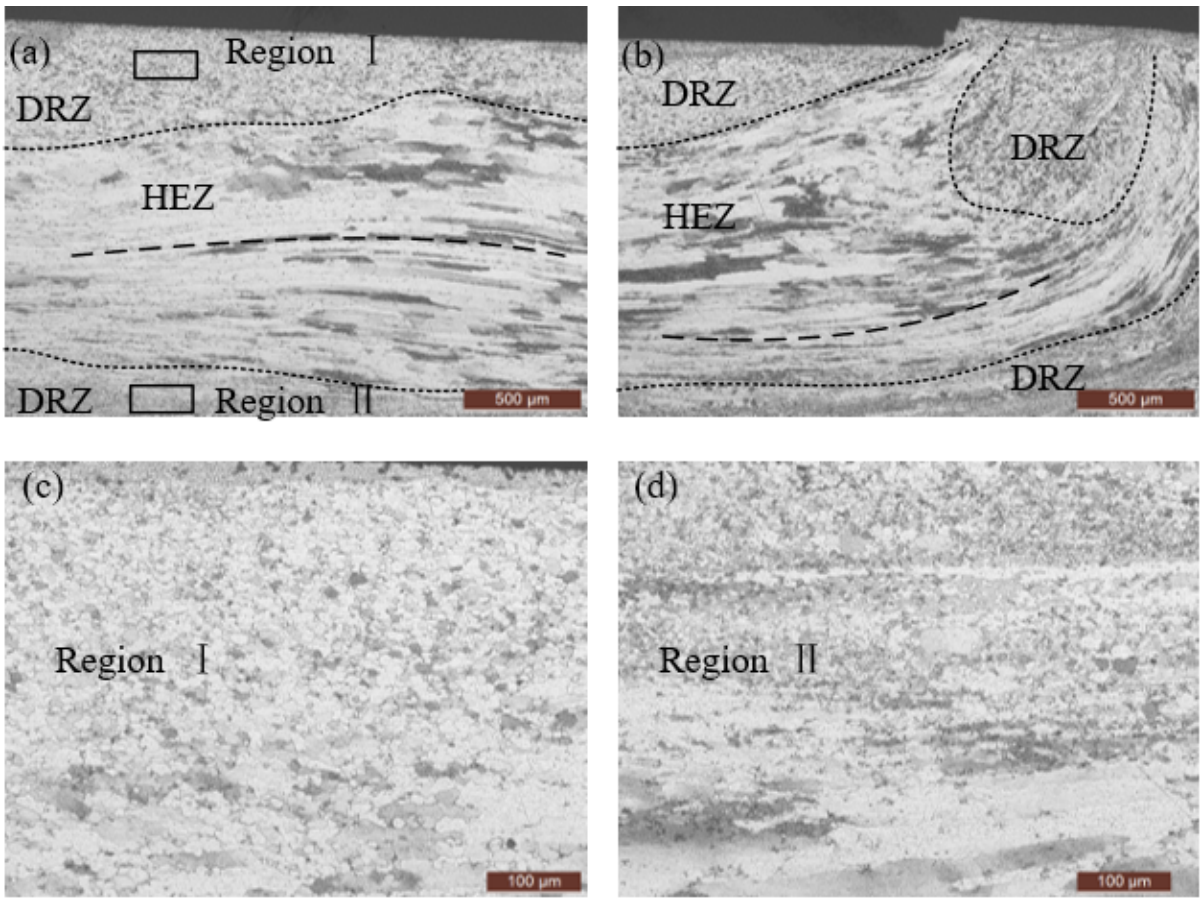

Fig. 6. HEZ/DRZ interface of joint under the plunge depth of 3 mm: (a) below the pin and (b) below the sleeve; (c) and (d) magnified views of Region I and Region II, as marked in Fig. 6a

Fig. 6 shows the HEZ/DRZ interface below the pin and sleeve of joint under the plunge depth of 3 mm. It is obvious that microstructures of HEZ at different locations present various morphologies, but the grains occur different levels of bending in different directions. The microstructures below the pin present arched grains (Fig. 6a), and those below the sleeve bend towards the moving direction of the sleeve (Fig. 6b). DRZ region enfolds the HEZ above and below the HEZ. The grains in DRZ are not obvious due to fine grain size. Regions I and II marked in Fig. 6a are magnified views of DRZ, as shown in Fig. 6c and 6d. The morphologies in DRZ at different regions both present small equiaxed grains.

3.3. Mechanical properties of RFSSW joint

Fig. 7 shows the microhardness distributions along the sleeve retreating path of RFSSW joints under different plunge depths. Three microhardness testing points were measured along the top surface of the cross section at each welding parameter. Each testing point is different distance from the top surface. Therefore, the X-axis represents the distance from the top surface. The actual microhardness indent marks are presented on the weld microstructure in Fig. 7. The microhardness value was obtained automatically by the Vickers hardness tester by calculating the diagonal length. The microhardness of the 2060 aluminum alloy is 100 HV. The microhardness values of this path are larger than those of the BM, which is associated with the fine equiaxed grains (Figs. 3f-3g). Under the same welding parameters, the microhardness values along sleeve retreating path fluctuate, but the fluctuation range is small. The microhardness

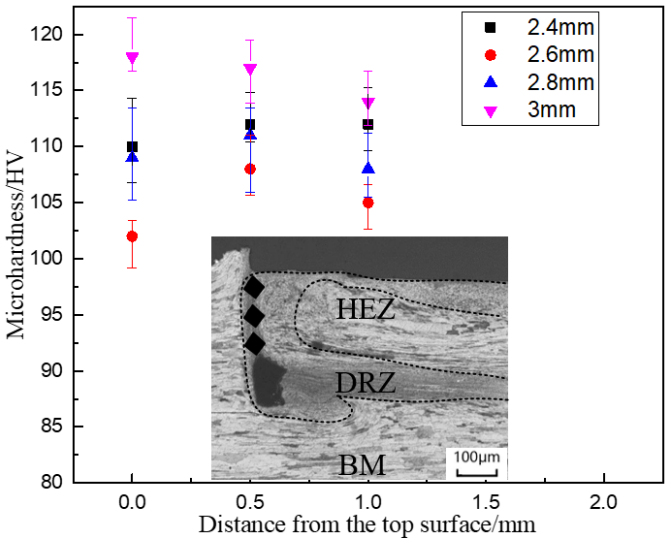

Fig. 7. Microhardness distributions in the sleeve retreating paths of joints under different plunge depths

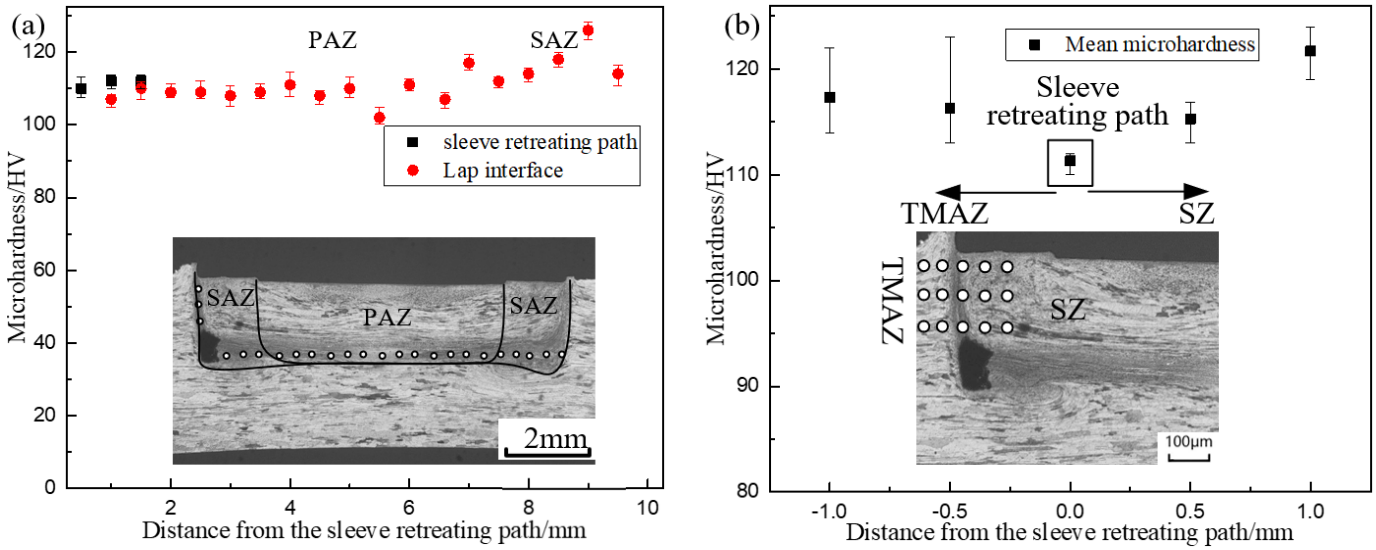

Fig. 8. Microhardness distributions of different regions in RFSSW joint under plunge depth of 2.8 mm: (a) the sleeve retreating path and the lap interface and (b) regions from TMAZ to SZ

values of joints under different plunge depths initially decrease and then increase with the increase of the plunge depth, and they are in the range of 100-120 HV.

Fig. 8a shows the microhardness distributions of the lap interface and the sleeve retreating path of the joint under the plunge depth of 2.8 mm. Thus, there are two hardness distribution curves. For one in the lap interface, the X-axis represents the distance away from void at the bottom of the SAZ. For one in the sleeve retreating path, the X-axis represents the distance from the void. The microhardness of the sleeve retreating path at each welding parameter is slightly larger than that in the lap interface, as shown in Fig. 8a. For the lap interface, the microhardness of the SAZ is slightly larger than that of the PAZ, and the microhardness of the PAZ is relatively stable. Fig. 8b shows the microhardness of regions from TMAZ to SZ. Testing range of points takes the testing points in sleeve retreating path in Fig. 8a as the center, and other testing points move 1 mm to both sides of the center testing points, as marked in Fig. 8b. The X-axis represents the distance from the sleeve retreating path. Three rows of hardness points were measured, and triplets of these points were averaged to regard as the microhardness values of regions along the thickness. Note that the microhardness values along the thickness were in the range of 110-125 HV. The sleeve retreating path is located at the middle of the measured region. Note that the microhardness value of the sleeve retreating path is lower than those values of TMAZ and SZ. However, the fluctuation of microhardness values was small. From the error bars of sample data, the variability of sample data is small for the single point (Figs. 7 and 8a). The microhardness values in Fig. 8b are averaged by three data from different points, and the variability of sample data are slightly larger than that of the single point.

Fig. 9 shows the tensile-shear loads of the RFSSW joints under different plunge depths. The maximum mean value of 5.71 kN is attained under the plunge depth of 2.4 mm. When the plunge depth gradually increases, the tensile-shear load of joint mainly presents a decreasing tendency. The tensile-shear load of joint under the plunge depth of 2.8 mm decreases to the minimum value, and then the mean tensile-shear load of joint starts to increase with the increase of the plunge depth. From the error bars of different loads, the variability of sample data is smaller at low plunge depths (2.4 mm and 2.6 mm) than that at high plunge depths (2.8 mm and 3 mm). However, the fluctuation of the mean tensile-shear load is small, and the loads are in the range of 5.1 kN-5.8 kN.

From the size of single void, the joint containing a large void (Fig. 4a) has the largest tensile-shear load. From the viewpoint of hook morphology, the largest tensile-shear load of joint has the smallest hook height, and the joint with downward hook has a larger tensile property than that with upward hook. From the viewpoint of microhardness value, the joint with the maximum microhardness in the sleeve retreating path do not obtain the

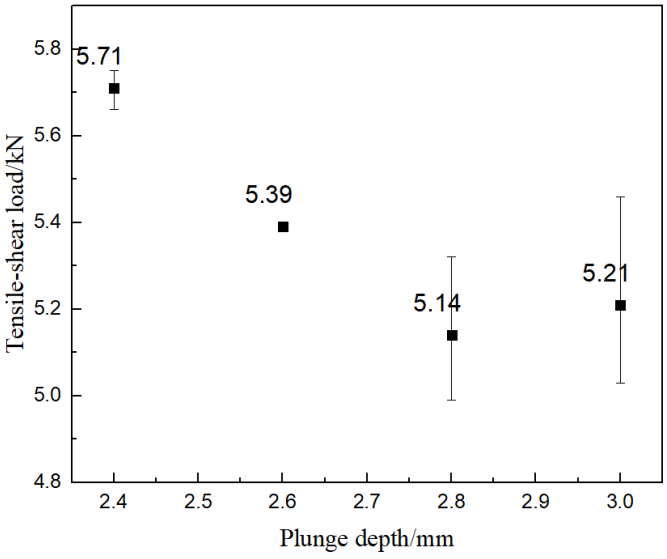

Fig. 9. Tensile-shear loads of joints under different plunge depths

largest tensile-shear load. Hence, hook morphology rather than void has an important influence on the tensile-shear property of joint, and the tensile-shear loads of joints with different void sizes have almost no difference.

Fig. 10 shows the macrographs of tensile-shear specimens after fracture. The fracture modes of tensile-shear specimens are similar and present shear-plug modes. The cracks propagate along the path of the sleeve retreating under the exterior load, and welding spot is retained on the lower plate.

Fig. 11 shows the fracture paths of tensile-shear specimens under the plunge depths of 2.4 and 2.6 mm. The void is still obvious in the fracture location corresponding to that in the cross section demonstrating the stability of the welding process. During the tensile-shear test, bending hook becomes the stress concentration point, and then the generated cracks have the tendency of propagating along the lap interface or the sleeve retreating path. Void separates the hook from the lap interface and decreases the bearing-load area along the sheet thickness. Furthermore, the defect-free lap interface (Fig. 5) increases the bonding strength of joint. Although the microhardness values of the sleeve retreating path are larger than those of the lap interface, the microhardness fluctuation of the zones from the TMAZ to the SAZ (Fig. 8b) causes the inconsistent deformation. These three above-mentioned reasons make the cracks propagate along the sleeve retreating path. Hence, although the void occurs near the tip of the hook, the void has no obvious influence on the tensile-shear load of joint when the plunge depth is reasonably selected.

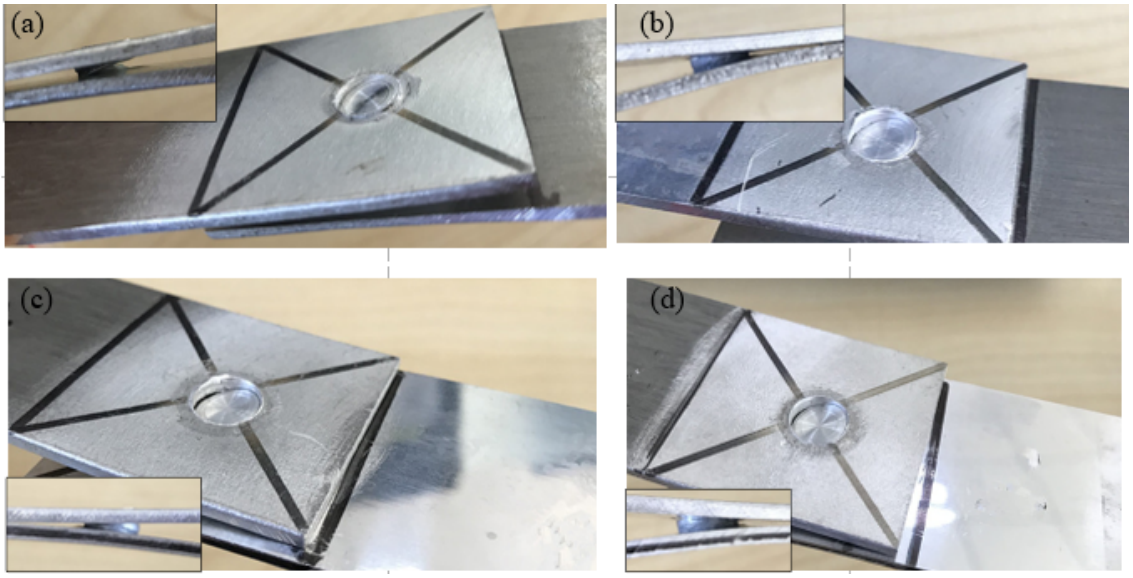

Fig. 10. Fracture modes of joints under different plunge depths: (a) 2.4, (b) 2.6, (c) 2.8 and (d) 3 mm

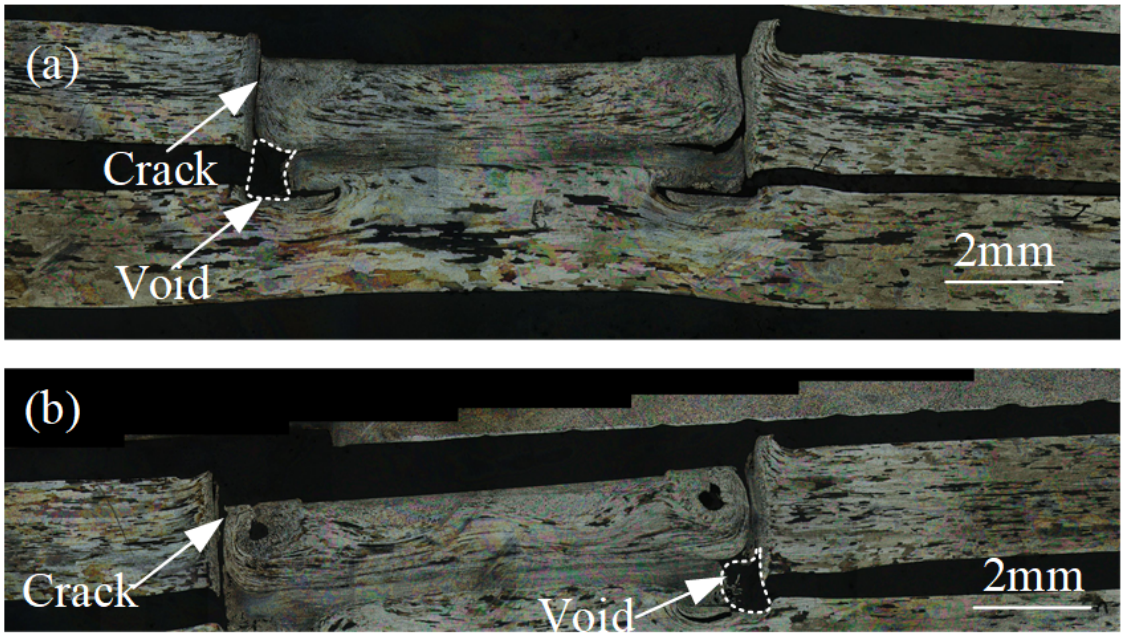

Fig. 11. Fracture paths of tensile-shear specimens under different plunge depths: (a) 2.4 and (b) 2.6 mm

4. Conclusions

RFSSW was used to weld 2 mm thick 2060 aluminum alloys. The formation, defect characteristics and mechanical properties of RFSSW joints under different plunge depths were investigated. The following conclusions can be drawn.

(1) The SZ of RFSSW joint is divided into DRZ and HEZ in accordance with the difference in microstructures. The microstructures of DRZ present fine equiaxed grains. HEZ consists of deformed and elongated lath-shaped grains, and the microstructures of different locations are characterized by deformed grains with various levels and directions.

(2) Void is observed near the hook tip when the plunge depth varies from 2.4 to 3 mm, and the size of single void decreases with the increase of the plunge depth. Hook bends downward when the plunge depth increases from 2.4 to 2.8 mm. Its height increases with increasing the plunge depth. However, the hook bends upward under the plunge depth of 3 mm.

(3) The hook height rather than void near the hook tip has an important influence on the tensile-shear load of joint. The tensile-shear load of joint initially decreases and then increases with increasing plunge depth, and the value is in the range of 5.1-5.8 kN. All the tensile-shear specimens present a shear-plug fracture mode.

Acknowledge

This work is supported by the National Natural Science Foundation of China (No. 51705339) and Aeronautical Science Foundation of China (No. 20171125002).

REFERENCES

[1] E.A. Starke, J.T. Staley Prog. Aerospace Sci. **32** (2-3), 131-172 (1996).

[2] R.S. Xiao, X.Y. Zhang, J. Manuf. Process. **16** (2), 166-175 (2014).

[3] R.K. Gupta, N. Nayan, G. Nagasireesha, S.C. Sharma, Mat. Sci. Eng. A. **420** (1-2), 228-234 (2006).

[4] C. Sharma, D.K. Dwivedi, P. Kumar, Int. J. Adv. Manuf. Tech. **81** (5-8), 1419-1431 (2015).

[5] K. Shukla, W.A. Baeslack, Sci. Technol. Weld. Joi. **14** (4), 376-387 (2009).

[6] K. Shukla, W.A. Baeslack, Scripta Mater. **56** (6), 513-516 (2007).

[7] P. Lacki, W. Wieckowski, P. Wieczorek, Arch. Metall. Mater. **60** (4), 2297-2306 (2015).

[8] P. Lacki, A. Derlatka, T. Galaczynski, Arch. Metall. Mater. **62** (1), 443-449 (2017).

[9] T. Pan, M. Santella, N. Blundell, SAE Int. J. Mater. Manuf. **2** (1), 23-29 (2009).

[10] M.K. Kulecki, Arch. Metall. Mater. **59** (1), 221-224 (2014).

[11] C.D. Castro, A.H. Plaine, N.G. de Alcântara, J.F. dos Santos, Int. J. Adv. Manuf. Tech. **99** (5-8), 1927-1936 (2018).

[12] M.D. Tier, T.S. Rosendo, J.F.D. Santos, N. Huber, J.A. Mazzaferro, C.P. Mazzaferro, T.R. Strohaecker, J. Mater. Process. Tech. **213** (6), 997-1005 (2013).

[13] Y. Shi, Y.M. Yue, L.G. Zhang, S.D. Ji, Y. Wang, T. Indian I. Metals. **71** (1), 139-145 (2018).

[14] Y. Yue, Y. Shi, S. Ji, Y. Wang, Z.W. Li, J. Mater. Eng. Perform. **26** (10), 5064-5071 (2017).

[15] J.Y. Cao, M. Wang, L. Kong, L.J. Guo, J. Mater. Process. Tech. **230**, 254-262 (2016).

[16] Y.H. Yin, N. Sun, T.H. North, S.S. Hu, Mater. Charact. **61** (10), 1018-1028 (2010).

[17] H. Badarinarayan, Q. Yang, S. Zhu, Int. J. Mach. Tool Manu. **49** (2), 142-148 (2009).

[18] B. Parra, V.T. Saccon, N.G.D. Alcântara, T. Rosendo, J.F. Santos, Tecnologia Em Metalurgia Materiais E Mineraã§ã£o. **8**, 184-190 (2011).

[19] Z.K. Shen, X.Q. Yang, S. Yang, Z.H. Zhang, Y.H. Yin, Mater. Design. **54** (2), 766-778 (2014).

[20] Z.K. Shen, X.Q. Yang, Z.H. Zhang, L. Cui, T.L. Li, Mater. Design. **44**, 476-486 (2013).